Electronic Supplementary Material (ESI) for Lab on a Chip.

Supplementary Information for

"A Low-Cost Smartphone Based Platform for Highly Sensitive Point-of-Care Testing with Persistent Luminescent Phosphors"

Andrew S. Paterson,[†ψ] Balakrishnan Raja,[†ψ] Vinay Mandadi,[‡ψ] Blane Townsend,[ψ] Miles Lee,[ψ] Alex Buell,[*] Binh Vu,[†] Jakoah Brgoch,[§] Richard C. Willson[†,≠,||]

†Department of Chemical & Biomolecular Engineering, University of Houston
ψ Luminostics, Inc., Houston, TX
‡Department of Mechanical Engineering, University of Houston
*Department of Computer Science, University of Houston
§Department of Chemistry, University of Houston
≠Department of Biology & Biochemistry, University of Houston
|| Centro de Biotecnología FEMSA, Tecnológico de Monterrey, Campus Monterrey

*Corresponding author: Ph.:+1 713-743-4308;
Fax: +1 713-743-4323
E-mail: willson@uh.edu

Conceptual Design of Smartphone Testing Attachment

The conceptual design of the smartphone attachment is illustrated in Figure S-1(A). The result window of the test cartridge contains the test line and control line regions of the membrane and lines up with the smartphone's back camera as shown in Figure S-1(B). In the present work the analyte and phosphors were mixed and directly applied to the strip's sample pad without use of a conjugate release pad.

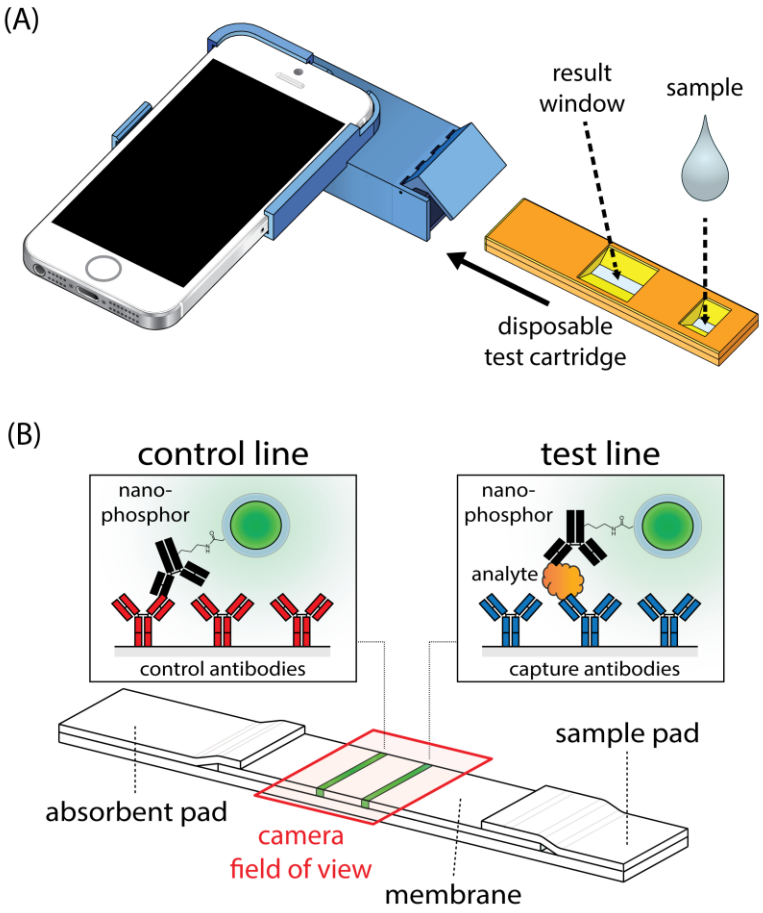

Figure S-1. (A) Illustration of smartphone attachment and LFA cartridge. (B) Layout of typical lateral flow strip used in the experiments in the present work.

3D Printing and Assembly of Smartphone Attachment

The 3D-printed parts of the attachment and their corresponding part numbers are listed in Figure S-2, along with an exploded view of the attachment. The main platform or attachment base (Part 1), was designed with features to facilitate easy sliding of the complete attachment onto the smartphone in a manner similar to a protective case. The fiber optics holder (Part 2) was glued onto the attachment base, and then packed with optical fibers as described in Materials and Methods. The lens holder (Part 3) was then inserted into the attachment. A single 7 mm diameter plano-convex lens was then glued into the lens holder with the planar surface oriented towards the smartphone camera. Two cartridge braces (Part 5) were printed and glued into the cartridge holder (Part 4) to keep the lateral flow test cartridge in the correct position when inserted into the attachment, and then the cartridge holder was glued onto the attachment base. A revolving door (Part 7) was connected to a door mount (Part 6) using 0.017 gauge wire, and then the assembled door module was glued onto the rest of the assembled parts to complete the attachment.

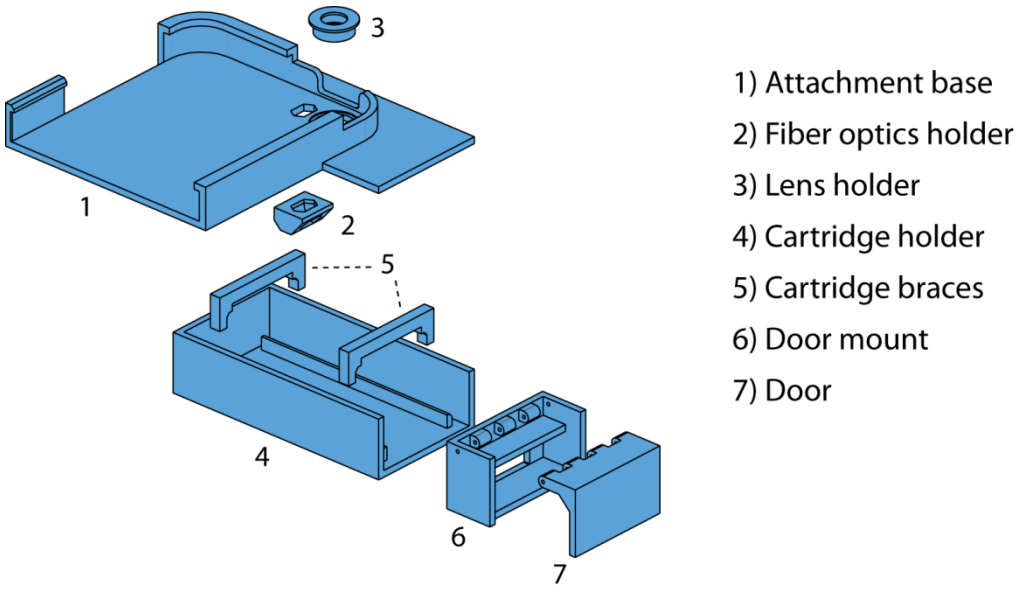

Figure S-2. Exploded view of the 3D printed parts in the iPhone 5s LFA reader.

In later version of the attachment a concave mirror that encircles the lens' optical axis, enclosing both the sensing region of the lateral flow strip and the fiber optics module, was added to make the illumination more uniform and better focus light onto the membrane. A rendering of the back side of a version of the attachment base with a concave mirror is shown in Figure S-3. For simplicity, the concave surface was made reflective by simply lining it with aluminum foil. The concave mirror could easily be mass produced with standard methods for fabricating plastic mirrors such as injection molding followed by surface metallization with silver using standard, low-cost processes such as electroless plating.

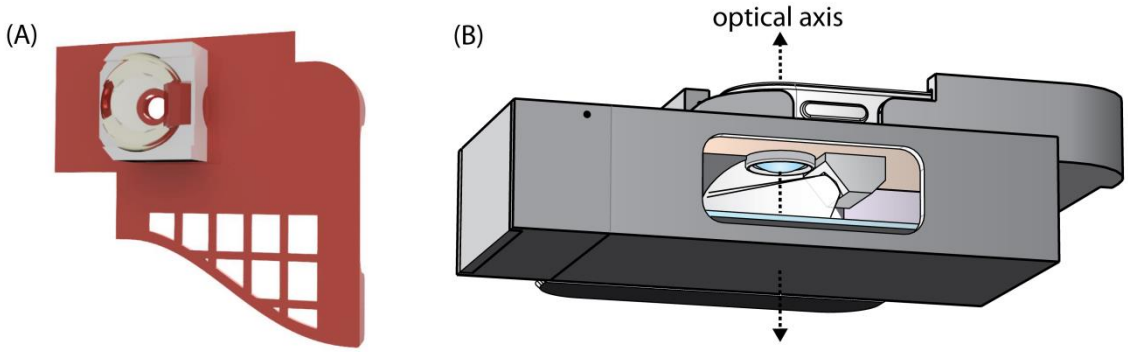

Figure S-3. (A) Photorealistic rending of concave mirror added to the attachment to enclose the sensing region and the fiber optics module for improved illumination. (B) Illustration showing cutaway of attachment and concave mirror during excitation with the smartphone camera flash.

Lateral Flow Strip Edge Detection

An important component in automated analysis of the lateral flow strip images on the smartphone is determining where the strip edges are located, as even with precise manufacturing tolerances small variations in the strip position by as little as 0.1 mm result in a shift by about ≈25 pixels in the camera's field of view. We developed a robust algorithm to automatically find the locations of the strip edges. First, the average intensity profile oriented along the width of the strip (the x-direction in Figure S-4) is calculated. This raw profile is smoothed to reduce noise, and then the first and second derivatives of the smoothed profile are calculated to find the inflection points in the profile. The inflection points of steepest ascent and descent correspond to the edges of the strip. The image is then cropped for analysis, with cropping boundaries specified by a small offset from the inflection points to reduce edge effects on the subsequent analysis.

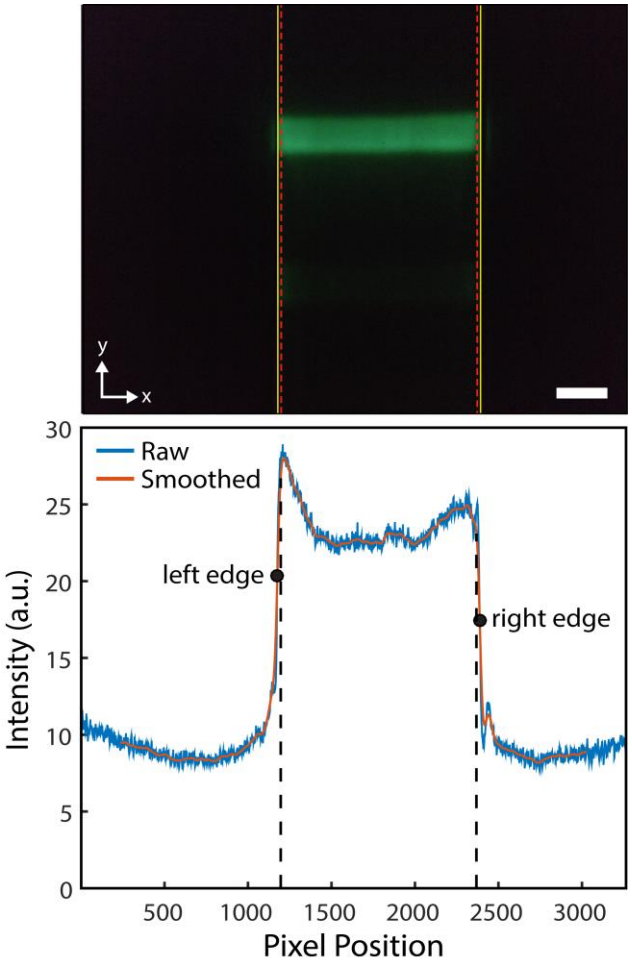

Figure S-4. (Top) Image of a lateral flow strip, with yellow lines marking strip edges and red dashed lines showing cropping boundaries. (Bottom) Intensity profile of the image along the x-direction, with inflection points corresponding to strip edges marked with black dots, and cropping boundaries denoted by dashed lines (scale bar = 1 mm).

Flash Emission Spectral Overlap with Phosphor Excitation

The emission spectrum of the iPhone 5s rear camera flash has the characteristic spectral profile of an InGaN LED, with a 450 nm emission peak and a cerium-doped yttrium aluminum garnet phosphor for downconverting some fraction of the InGaN blue light to produce an overall white light spectrum (Figure S-5). The excitation spectrum of $SrAl_2O_4$: Eu^{2+}, Dy^{3+} has a maximum near 365-370 nm, and tails off towards longer wavelengths above ≈425 nm into the blue region of the electromagnetic spectrum. The spectral overlap of the $SrAl_2O_4$: Eu^{2+}, Dy^{3+} excitation with the flash emission is relatively small, and might suggest the strontium aluminate nanophosphors would not be effectively excited by the flash. However, Eu^{2+}-doped strontium aluminate is a highly efficient phosphor with quantum yields above 90%, and is used in glow-in-the-dark products that are intended to be excited by typical indoor white light sources. Furthermore, the design of the smartphone attachment maximizes the irradiance of the phosphors in the sensing region of the strip, which helps compensate for the non-optimal spectral overlap.

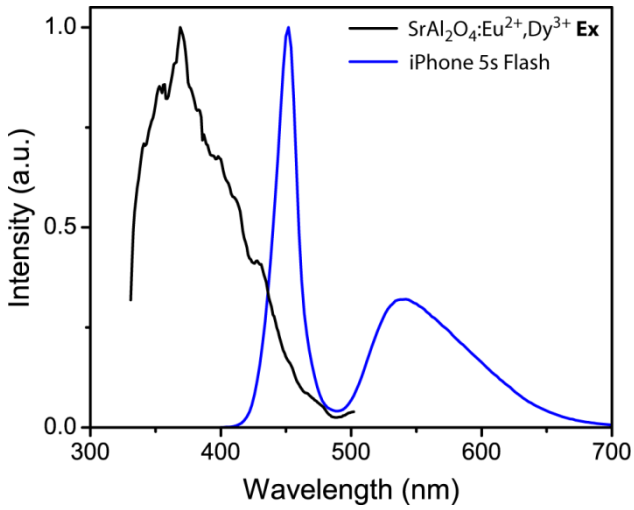

Figure S-5. Excitation spectra of $SrAl_2O_4$: Eu^{2+}, Dy^{3+} phosphors overlaid with iPhone 5s rear camera flash emission spectrum.

Detection Limit of Persistent Luminescence Nanoparticles

The combination of image averaging and line scan averaging enhances the detectability of the phosphors. Figure S-6 shows the resulting profiles from images of membranes spotted with lines of phosphors at decreasing concentrations. The amount of phosphors dispensed per pixel was calculated using the head speed of the dispenser, the concentration and volumetric flow rate of phosphors being dispensed, and the number of pixels corresponding to the region where the phosphors were dispensed. The line with ≈65 fg of phosphors/pixel is detectable above the background. From the Archimedes single-particle mass distribution reported previously[35] with an average particle mass of 50 fg, this indicates that a line on a membrane containing an average of ≈1-2 nanophosphors per pixel would be detectable with the smartphone imaging platform.

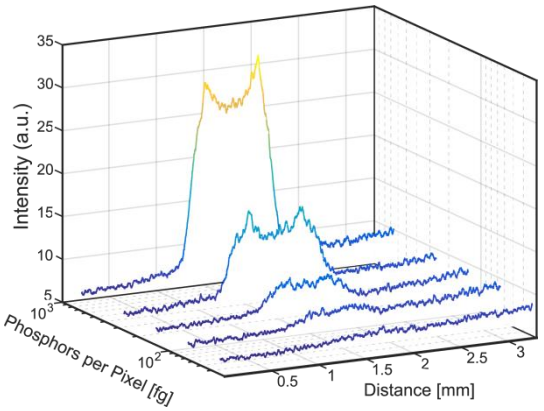

Figure S-6. Average line scan down the length of a strip spotted with nanophosphors. (9 averaged images acquired with torch only, no flash for excitation).

Excitation and Time Delay Control

Smartphone LEDs can be operated either in continuously-on "torch" mode or in "flash" mode, in which the LED produces a brief, intense pulse of light. Figure S-7 shows LED intensity as a function of time when using a 3 s torch followed by a single flash. On the iPhone 5s, the duration of the flash cannot be adjusted, and was measured to consistently last approximately 300 ms. Note that brief low-intensity illumination period that occurs at around 4 s in Figure S-7 is part of the flash process. The light intensity from the LED is significantly higher in flash mode than torch mode, so the flash was used in combination with the torch to more effectively excite the nanophosphors.

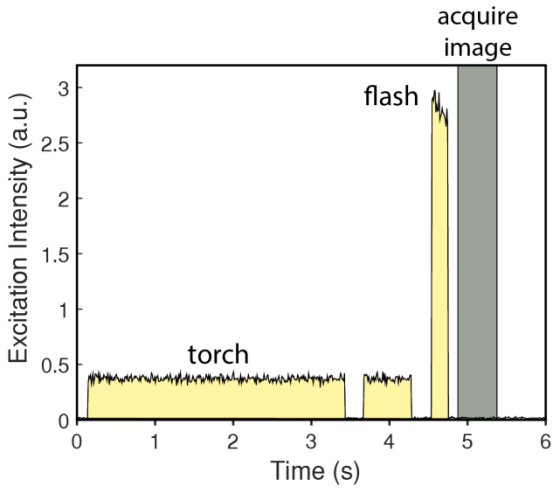

Figure S-7. Relative intensity of the iPhone 5s torch and flash, measured with a 3x3 mm Hamamatsu multi-pixel photon counter through a pinhole. The dark shaded region marks image acquisition after a ≈100 ms time delay time with a 0.5 s exposure time.

A sequence of frames from an imaging cycle of a lateral flow strip is shown in Figure S-8. First, the strip is illuminated and the smartphone camera is allowed to autofocus on the strip. The focus is locked and the torch is then set to the maximum allowable intensity for a few seconds, after which a single flash is triggered. The camera settings are then configured to the maximum exposure time and ISO setting, and the first post-flash frame is captured and stored for processing and signal quantitation.

Time stamp data collected while running the app indicated a time delay between the flash and image acquisition on the order of 100 ms. Due to the multi-exponential decay kinetics of persistent luminescence, a shorter time delay between excitation and imaging could significantly improve detection of the nanophosphors, and should be technically feasible with the hardware and image sensors in current generation smartphones. However, implementing control over the device with sub-millisecond time delays would likely require programming the app at a deeper level with more control than is currently permitted with the available APIs. Additionally, increasing the duration of the more intense flash could further enhance sensitivity.

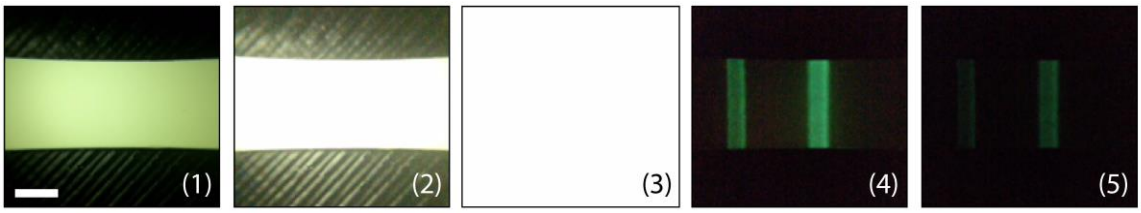

Figure S-8. Sequence of frames captured of strip run with 0.73 ng/mL hCG with the imaging app showing (1) initial autofocus, (2) excitation with torch, (3) excitation with flash, (4) first post-flash frame captured of the persistent luminescence, and (5) a darker subsequent frame captured ≈5 seconds after the flash. (scale bar = 2 mm).

FluorChem Image Analysis

A head-to-head comparison of the detection limits and dose response curves for the intensity ratio I_{TL}/I_{CL} as a function of hCG concentration was carried out with the smartphone platform and FluorChem CCD gel imaging system to evaluate the relative sensitivity, signal variability, and linearity of the image data acquired with the two systems.

For a fairer comparison of the smartphone platform and the FluorChem, an algorithm was written to automate analysis of images of lateral flow strips acquired with the FluorChem. Immediately after capturing a luminescence image of a set of strips, a brightfield image is captured. Intensity profile analysis of the brightfield image, similar to that used for detection of the LFA strip edge positions with the smartphone platform, is used to find key inflection points that correspond to the positions of the top and bottom edges of the strips, the overlap regions of the absorbent pad and sample pad onto the membrane, and the side edges of the membrane. A brightfield image with these positions marked with colored lines is shown in Figure S-9(A). The red rectangles outline the boundaries of the membrane for each strip, and are used to analyze luminescence from the strips individually (Figure S-9(B)). The membrane region of each strip is further divided into two separate regions, one containing the control line and the other containing the test line. A rectangle of fixed height, approximately equal to the test line and control line thickness, is translated vertically within both the test line and control line region, and the average pixel intensity within the rectangle is calculated as a function of position. The rectangle position with maximum average pixel intensity corresponds to the test line or control line, as shown in Figure S-9(C).

The dose response curve of I_{TL}/I_{CL} as a function of hCG concentration for the strips imaged with the FluorChem is shown in Figure S-10. Linear interpolation between the concentrations bracketing the $\mu + 3\sigma$ cutoff indicate a detection limit near ≈75 pg/mL, which was slightly worse than the 45 pg/mL detection limit determined with images of the same LFA strips acquired with the iPhone 5s and analyzed using a similar method. A major reason for the better detection limit with the iPhone 5s than the FluorChem is imaging lag. With the FluorChem, the strips are excited under a UV lamp then manually inserted into the instrument for imaging. The time delay between excitation and imaging is at least ≈5 s, although the CCD exposure time is 720 times longer at 6 minutes compared to 0.5 s. Additionally, the higher magnification of the smartphone attachment with the phone distributes the light over more pixels, so the calculated

pixel intensities with the iPhone 5s images may be less prone to variations from shot noise than the FluorChem. This effect is observable in the images in Figure S-11, which show side-by-side comparisons of the FluorChem and iPhone 5s images scaled to the same size, with more apparent random noise in the FluorChem images.

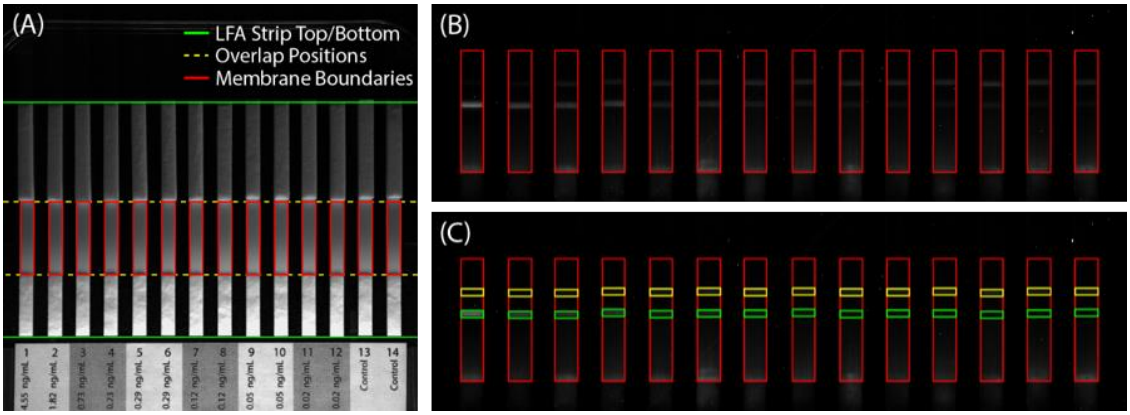

Figure S-9. Algorithm for FluorChem image analysis. (A) Brightfield image for detecting strip boundaries and overlap positions. (B) Membrane regions in luminescence image. (C) Positions of Control Line (yellow) and Test Line (green). Each strip is 4 mm wide.

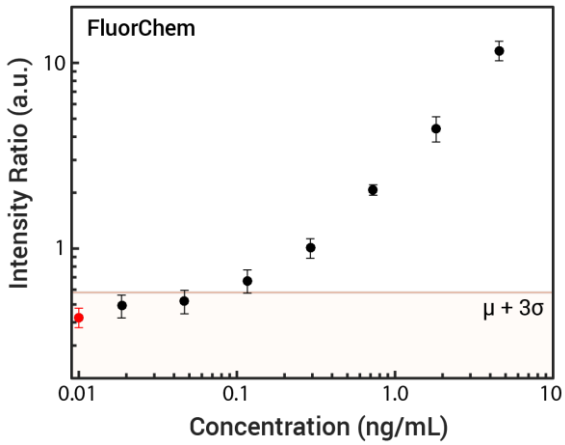

Figure S-10. Serial dilution of hCG detected with FluorChem. Horizontal line marks the mean of the blank plus three standard deviations. The leftmost point on the plot corresponds to the no-target controls, and was marked red to distinguish it from the black data points which correspond to the positive samples spiked with different concentrations of hCG.

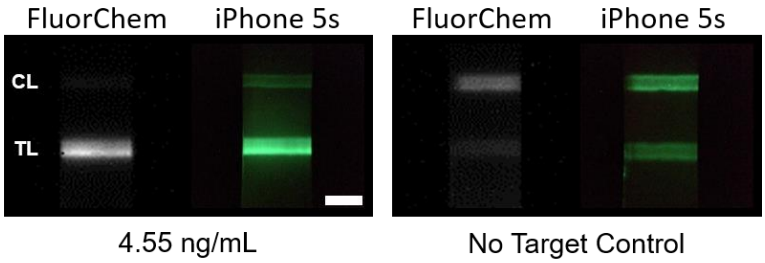

Figure S-11. Comparison of images of the same strip acquired with the FluorChem and iPhone 5s at 4.55 ng/mL hCG and a blank with no hCG (scale bar = 2 mm).